Major Groove (*R*)-α-(*N*^{6}-Adenyl)styrene Oxide Adducts in an Oligodeoxynucleotide Containing the Human *N-ras* Codon 61 Sequence: Conformations of the R(61,2) and R(61,3) Sequence Isomers from ^{1}H NMR†

Binbin Feng,‖ Liang Zhou,‡ Mariella Passarelli,§ Constance M. Harris, Thomas M. Harris, and Michael P. Stone*

Center in Molecular Toxicology and Department of Chemistry, Vanderbilt University, Nashville, Tennessee 37235

Received December 28, 1994; Revised Manuscript Received July 25, 1995⊗

ABSTRACT: Conformations of (*R*)-α-(*N*^{6}-adenyl)styrene oxide adducts at positions X^6 in d(CGGACXA-GAAG)·d(CTTCTTGTCCG) and X^7 in d(CGGACAXGAAG)·d(CTTCTTGTCCG), incorporating codons 60, 61 (underlined), and 62 of the human *n-ras* protooncogene, were refined from ^{1}H NMR data. These were the R(61,2) and R(61,3) adducts. Chemical shift perturbations were in the 5′-direction from the sites of adduction; large changes were observed for C^5 H5 and H6 in the R(61,2) adduct. The styrene moieties were only partially defined by NOE data. Spectral overlap, particularly for the R(61,2) adduct, prevented complete assignments of the aromatic resonances; likewise, there were insufficient data to orient the CH_2OH moieties. Ring flips were slow on the NMR time scale. For the R(61,2) adduct 260 restraints were obtained from NOE data at three mixing times using relaxation matrix analysis; for the R(61,3) adduct 230 restraints were obtained. Structures emergent from molecular dynamics/simulated annealing for the R(61,2) adduct converged to average and maximum pairwise rms differences of 1.3 and 1.7 Å, respectively, while those for the R(61,3) adduct converged to average and maximum pairwise rms differences of 1.2 and 1.6 Å. Sixth root residual indices of 7.5 and 6.8 × 10^{-2} were measured between the refined structures and NOE intensities using relaxation matrix calculations for the R(61,2) and R(61,3) adducts, respectively. The styrene rings were in the 5′-direction from the lesion sites in the major groove. The preferred orientation calculated for the R(61,2) adduct placed the styrene ring edgewise and approximately orthogonal to C^5, while that calculated for the R(61,3) duplex had the styrene ring approximately orthogonal to the major groove edges of base pairs A^6·T^{17} and $^{R\text{-}SO}$A^7·T^{16}.

Styrene is one of the top chemicals produced in the United States for the manufacture of various plastics and resins. Its toxicology (Bond, 1989) is of interest since it is mutagenic in both prokaryotic (de Meester et al., 1977; Wade et al., 1978) and eukaryotic (Bonatti et al., 1978) test systems and possibly in humans (Ott et al., 1980; Hodgson & Jones, 1985; Matanoski & Schwarts, 1987; Wong, 1990). Styrene induces sister chromosome exchange and aberrations in human lymphocytes *in vitro* (Norppa et al., 1980, 1981). The genotoxicity is believed to be due to cytochrome P_{450}-mediated metabolism to styrene oxide, SO[1] (Harris et al., 1986; Foureman et al., 1989; Elovaara et al., 1991; Guengerich et al., 1991; Guengerich, 1992; Nelson et al., 1993; Nakajima et al., 1994a,b). The oxide reacts to form adducts in nucleotides, including R- and S-adducts at the exocyclic amino groups of guanine and adenine (Savela & Hemminki, 1986), although the distribution of DNA adducts induced *in vivo* remains uncertain.

Current multistep progression models of tumorigenesis [reviewed by Cheng and Loeb (1993)] posit that cellular transformation occurs as a consequence of multiple mutations which accumulate over time, some of which may be preexisting and some of which may be induced by exposure to endogenous or exogenous carcinogens. A difficulty with these models is that the occurrence of independent mutations necessary to induce transformation within a single cell seems statistically improbable. This apparent discrepancy could be explained if mutation frequencies are greater for specific DNA sequences, due to increased reactivities with chemical carcinogens (Muench et al., 1983; Refolo et al., 1985; Boles & Hogan, 1986; Marien et al., 1987; Benasutti et al., 1988; Kootstra et al., 1989; Moyer et al., 1989; Osborne, 1990; Dittrich & Krugh, 1991a,b; Margulis et al., 1993) or decreased probabilities of repair (Zarbl et al., 1985; Topal et al., 1986; Topal, 1988; Voigt et al., 1989; Voigt & Topal, 1990), or there exist mutator phenotypes (Loeb, 1991).

The formation of adducts between DNA and chemical carcinogens such as SO probably represents an early event in carcinogenesis (Miller, 1970). Protooncogene coding sequences represent genetic loci in which adduct-induced mutations can directly initiate cellular transformation. The *ras* protooncogene encodes a 21 kDa protein, p21, which functions with GTPase activity on the inner surface of the

† This research was supported by grants from the NIH, ES-05355 (M.P.S.) and ES-05509 (T.M.H.). Funding for the NMR spectrometer was supplied by a grant from the NIH shared instrumentation program, RR-005805, and the Vanderbilt Center in Molecular Toxicology, ES-00267.

* Author to whom correspondence should be addressed.

‖ Present address: Cellular Biochemistry and Biophysics Program, Memorial Sloan-Kettering Cancer Center, New York, NY 10021.

‡ Present address: Department of Pharmacology, 4 Research Court Cancer Section, Georgetown University, Rockville, MD 20850.

§ Present address: Department of Chemistry, University of Maine at Farmington, P.O. Box 976, Farmington, ME 04938.

⊗ Abstract published in *Advance ACS Abstracts,* October 1, 1995.

[1] Abbreviations: DNA, deoxyribonucleic acid; DSS, sodium 4,4-dimethyl-4-silapentanesulfonate; EDTA, ethylenediaminetetraacetic acid; HPLC, high-pressure liquid chromatography; MD, molecular dynamics; NMR, nuclear magnetic resonance; NOE, nuclear Overhauser enhancement; NOESY, two-dimensional NOE spectroscopy; ppm, parts per million; RMA, relaxation matrix analysis; SO, styrene oxide; TPPI, time-proportional phase increment; TOCSY, total homonuclear correlated spectroscopy; 1D, one dimensional; 2D, two dimensional.

0006-2960/95/0434-14021$09.00/0

plasma membrane and regulates signal transduction [reviewed by Barbacid (1987)]. Mutations within a limited number of codons in the p21 gene, including codon 61, cause oncogene activation. Evidence suggesting that chemical carcinogens induce mutations and thereby activate protooncogenes such as *ras* comes from comparison of mutations in carcinogen-induced tumors within a number of tissues to known or suspected reaction sites of specific carcinogens (Zarbl et al., 1985; Quintanilla et al., 1986; Vousden et al., 1986).

The *ras61* oligodeoxynucleotide, d(CGGACAAGAAG)·d(CTTCTTGTCCG),[2] contains the sequence for codons 60, 61 (underlined), and 62 of the human *n-ras* gene. Structural refinement suggested sequence-specific variations at codon 61 (Calladine, 1982), associated with the purine−pyrimidine (R−Y) step at $A^4 \cdot T^{19} \rightarrow C^5 \cdot G^{18}$ and the Y−R step at $C^5 \cdot G^{18} \rightarrow A^6 \cdot T^{17}$; these might modulate chemical reactivity at the codon 61 site (Feng & Stone, 1995). After adduction, sequence-specific structural perturbations in the adducted *ras61* oligodeoxynucleotide might modulate mutagenesis or damage repair (Cho et al., 1992, 1994; Eckel & Krugh, 1994a,b). A nonbiomimetic synthesis enabled large-scale production of site-specific (*R*)-α-(*N*^{6}-adenyl)-styrene oxide-modified *ras61* oligodeoxynucleotides, while simultaneously eliminating problems in controlling the regioselectivity of adduction. The enantiomeric phenylglycinol was reacted with oligodeoxynucleotides containing 6-chloropurine deoxyriboside at either the A^6 or the A^7 nucleotide within codon 61, affording the desired diastereomer of styrene oxide at either A^6 or A^7 after subsequent deprotection and purification (Harris et al., 1991). These sequence isomers were named the R(61,2) and R(61,3) adducts (Scheme 1). Replication studies revealed the R(61,2) R-SO adduct to be a kinetic block to replication for a number of bacterial and eukaryotic polymerases (Latham et al., 1995), including HIV-1 reverse transcriptase (Latham & Lloyd, 1994). The R(61,3) adduct, with the R-SO adduct moved one nucleotide downstream to the codon 61 wobble position, was bypassed during replication (Latham et al., 1995). This suggested differing DNA replication effects at the R(61,3) as opposed to the R(61,2) SO lesion.

This work compares solution conformations of the R(61,2) and R(61,3) adducts, obtained from ^{1}H NMR spectroscopy. Interproton distance constraints obtained from NOESY spectra were used to refine solution structures via restrained MD simulation with a simulated annealing protocol, followed by relaxation matrix back-calculation (Keepers & James, 1984; Havel & Wuthrich, 1985; Wuthrich, 1986; Nilsson et al., 1986; Borgias & James, 1990; Madrid et al., 1991). The structures which emerge from the calculations are in the B-family. The preferred conformation of the R(61,2) adduct is similar, but not identical, to that of the R(61,3) oligodeoxynucleotide. In both instances, structural perturbations are confined to the base pairs at and immediately adjacent to the site of adduction. In both, the styrene phenyl ring is located in the major groove and oriented toward the 5′-direction from the site of adduction. For the R(61,2) adduct, the plane of the phenyl ring is predicted to prefer an edgewise alignment in the major groove, while for the R(61,3) adduct, the preferred alignment is predicted to have the plane of the phenyl ring on the floor of the groove. The refined structures suggest greater steric hindrance in locating the styrenyl ring in the major groove adjacent to the 5′-neighbor nucleotide C^5 in the R(61,2) adduct as compared to the 5′-neighbor A^6 in the R(61,3) adduct. This may be reflected in the kinetics of nucleotide insertion and strand elongation in the R(61,2) adduct as compared to the R(61,3) adduct, suggesting differences in the manner in which these two adducts interact with the replication complex.

Scheme 1: R(61,2) and R(61,3) Oligodeoxynucleotides, Where X = the (*R*)-α-(*N*^{6}-Adenyl)styrene Oxide Adduct and (Bottom) Structure of the (*R*)-α-Styrene Oxide Adduct at Adenine N^6 and Designations of the Styrene Protons

ras codons

60 61 62

5′-C^1 |G^2 G^3 A^4 |C^5 X^6 A^7 |G^8 A^9 A^{10}|G^{11}-3′

3′-G^{22}|C^{21}C^{20}T^{19}|G^{18}T^{17}T^{16}|C^{15}T^{14}T^{13}|C^{12}-5′

ras codons

60 61 62

5′-C^1 |G^2 G^3 A^4 |C^5 A^6 X^7 |G^8 A^9 A^{10}|G^{11}-3′

3′-G^{22}|C^{21}C^{20}T^{19}|G^{18}T^{17}T^{16}|C^{15}T^{14}T^{13}|C^{12}-5′

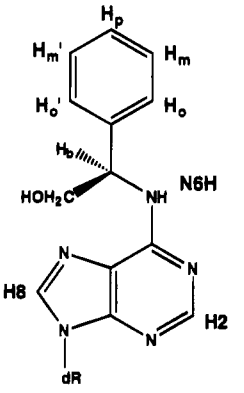

MATERIALS AND METHODS

Sample Preparation. The oligodeoxynucleotide d(CTTCTTGTCCG) was purchased from the Midland Certified Reagent Co. (Midland, TX). The concentration of the single-stranded unmodified oligodeoxynucleotide was determined from the extinction coefficient of 9.08×10^4 M^{-1} cm^{-1} at 260 nm (Borer, 1975). To construct the R(61,2) and R(61,3) α-SO-adducted duplexes, equal molar amounts of either the R(61,2) or R(61,3) strands (Harris et al., 1991), respectively, and the unmodified complementary strand were mixed in 10 mM NaH_2PO_4, 0.1 M NaCl, and 50 μM Na_2EDTA at pH 6.9. In each case, the annealed duplex was eluted from a hydroxylapatite column using sodium phosphate and desalted by gel filtration using Bio-Gel P-2 (Bio-Rad Laboratories, Richmond, CA). NMR samples were prepared in 0.1 M NaCl, 0.01 M NaH_2PO_4, and 0.05 mM Na_2EDTA (pH 7.4). For observation of nonexchangeable protons, NMR samples were repeatedly lyophilized and dissolved in

[2] The oligonucleotides discussed in this paper do not have terminal phosphate groups—we abbreviate the nomenclature for oligonucleotides by leaving out the phosphodiester linkage. A, C, G, and T refer to mononucleotide units. A superscript to the right refers to the numerical position in the oligonucleotide sequence starting from the 5′-terminus of chain A and proceeding to the 3′-terminus of chain A and then from the 5′-terminus of chain B to the 3′-terminus of chain B. C2, C5, C6, C8, C1′, C2′, C2″, etc. represent specific carbon nuclei. H2, H5, H6, H8, H1′, H2′, H2″, etc. represent the protons attached to these carbons.

0.5 mL of 99.996% D_2O, giving a 2 mM solution. For assignments of water-exchangeable protons, samples were dissolved in a 9:1 H_2O-D_2O buffer of the same composition as described above.

NMR Spectroscopy. Spectra were recorded at a ^1H frequency of 500.13 MHz. The data were processed using FELIX 2.3 (Biosym Technologies, San Diego, CA), running on Iris or Indigo workstations (Silicon Graphics, Inc., Mountain View, CA). Phase-sensitive NOESY spectra in D_2O were recorded using the standard pulse sequence and the TPPI method for phase cycling; the mixing time was 250 ms. The residual water resonance was saturated during the relaxation delay and the mixing period. The NOESY pulse program was modified to eliminate artifacts from zero-quantum coherence and *zz* terms at short mixing times. A systematically shifted composite 180° pulse was implemented within the mixing period, and composite 90° pulses were used in place of the second and third 90° pulses in the standard pulse sequence (Bodenhausen et al., 1984). TOCSY experiments used the standard pulse sequence with a 100 ms MLEV-17 spin-lock field (2 G). Chemical shifts were referenced internally relative to DSS. One-dimensional experiments in 90% H_2O used a 1-1 echo pulse sequence (Plateau & Gueron, 1982). Two-dimensional phase-sensitive NOESY experiments in 90% H_2O used the 1-1 sequence as the read pulse (Bax et al., 1987; Sklenar et al., 1987), at 20 °C. Convolution difference used during processing minimized the residual water signal (Marion et al., 1989). The mixing time was 250 ms.

Relaxation Matrix Analysis. For the R(61,2) duplex, NOESY experiments were run at mixing times 150, 200, and 250 ms, while for the R(61,3) duplex, NOESY experiments were run at mixing times 100, 150, and 250 ms. Footprints were selected manually with FELIX 2.3 to fit NOE cross-peaks at the contour level which showed the weak NOEs but not random noise. For overlapped cross-peaks, footprints were estimated. NOE cross-peaks were volume integrated for the three spectra using the same contour levels. For each of the three mixing times, a hybrid intensity matrix was constructed using MARDIGRAS (Borgias & James, 1990). RMA calculations were performed on each matrix, yielding three sets of internuclear distances. The distances were averaged, and error bounds were calculated to provide the restraints used in MD calculations. Some calculated distances, primarily involving sugar protons, were not included as restraints in MD calculations since the estimated error in their measurement exceeded the range of distances physically possible between the two protons in the covalent structure of the oligodeoxynucleotide. Individual distance restraints calculated by MARDIGRAS to be greater than 5 Å were removed from the distance restraint set. Additional restraints were removed if they were found to be inconsistent with a reasonable structure. In general, these difficulties were due to errors in intensity measurements arising from spectral overlap or from cross-peaks close to the water resonance whose intensities were altered by the water presaturation pulse used during acquisition of NOESY spectra. An isotropic correlation time τ_c of 5 ns was used for both sugar and base protons.[3]

[3] This was based on τ_c measured from a fluorescence anisotropy study of an 11-*mer* oligodeoxynucleotide adducted with benzo[*a*]pyrene (Dr. Irene S. Zegar, personal communication).

Restrained Molecular Dynamics. INSIGHTII (Biosym Technologies, San Diego, CA) was used to build starting structures and for molecular visualization. Potential energy minimization and MD calculations were performed using X-PLOR (Brunger, 1992). The force field parameters for the $^{R\text{-}SO}$A nucleotide are collected in Figure S1 in the supporting information. The empirical energy function derived from the CHARMM force field (Brooks et al., 1983) and developed for nucleic acids treated hydrogens explicitly (Nilsson & Karplus, 1986). The nonbonded interactions included van der Waals and electrostatic terms, which used the pure Lennard-Jones and Coulomb functions, respectively. The electrostatic term was based on a reduced charge set of partial charges (−0.32/residue) and a dielectric constant of 4.0. The cutoff radius for nonbonded interactions was 11 Å, and the nonbonded list was updated if any atom moved more than 0.5 Å. The SHAKE algorithm (Ryckaert et al., 1977) fixed bond lengths involving hydrogens. The integration time step in the molecular dynamics calculations was 1 fs. Structure coordinates were archived every 0.1 ps. Back-calculation of NMR data was performed using CORMA (Keepers & James, 1984). The refined structures were analyzed using DIALS AND WINDOWS 1.0 (Ravishankar et al., 1989).

RESULTS

Spectral Assignments. Figure 1 shows the base-to-H1′ connectivities for the R(61,2) and R(61,3) duplexes. Non-exchangeable proton resonance assignments were made from NOESY and TOCSY spectra collected at 20 °C (Hare et al., 1983; Feigon et al., 1983). The remainder of the deoxyribose protons were assigned from TOCSY and NOESY spectra on the basis of the sequential assignments of the H1′ protons. The assignments of the H2′ and H2″ sugar protons were made from their NOEs with the H1′ sugar protons of the same residue on the basis of the assumption that, for a B-like DNA, the H1′-H2″ distances were shorter than the H1′-H2′ distances. Therefore, the stronger cross-peaks were assigned to the H2″ protons. The adenine H2 protons were assigned from weak cross-peaks to the H1′ protons of the adjacent 3′-nucleotides and from the strong cross-peaks to the imino protons of the complementary thymines. The signals for both duplexes were sharp and well resolved. In both strands, a complete set of sequential connectivities was observed. Tables 1S and 2S in the supporting information list the chemical shifts of the nonexchangeable protons for the R(61,2) and R(61,3) duplexes.

The notable features of both duplexes were the upfield chemical shifts of the base aromatic protons of the nearest neighbor nucleotide 5′ to the SO adduct. In the unmodified *ras61* oligodeoxynucleotide C^5 was shifted upfield, presumably due to increased stacking interactions since C^5 was flanked on both sides by adenine (Feng & Stone, 1995). The upfield shift of C^5 in the R(61,2) oligodeoxynucleotide was still greater. Likewise, in the R(61,3) duplex, A^6 H8 was shifted upfield as compared to its location in the unmodified *ras61* sequence (see section following regarding chemical shift perturbations). For both of these modified oligodeoxynucleotides, C^{12} H5 and H6, from the terminal C·G base pair, resonated downfield of the other cytosine H5 and H6 protons, which were clustered at 5.4−5.8 and 7.3−7.5 ppm, respectively. This clustering of the cytosine aromatic resonances was similar to that observed in the unmodified

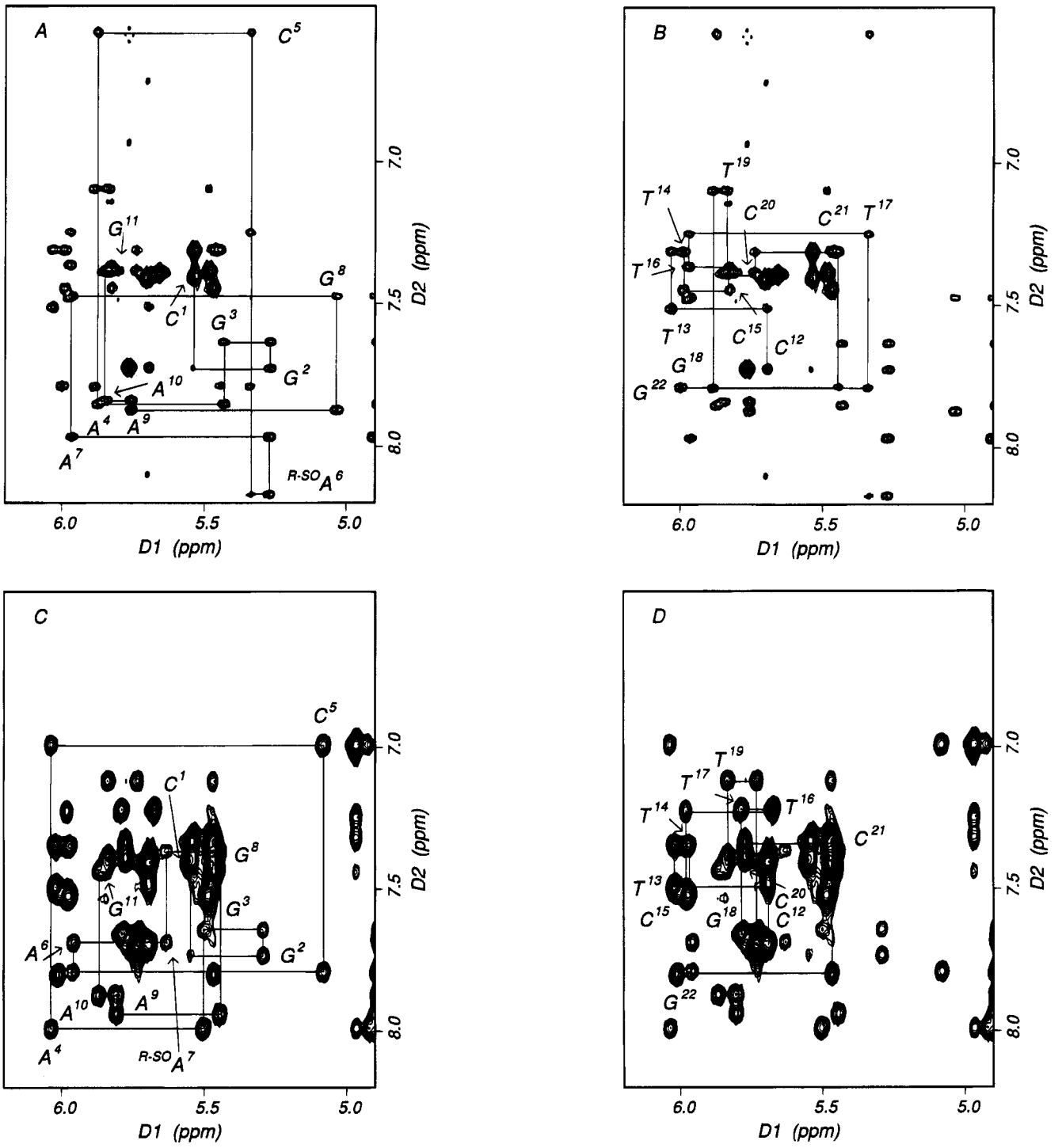

FIGURE 1: Expanded plot of a phase-sensitive NOESY spectrum in D_2O buffer with a mixing time of 250 ms showing the sequential NOEs from the aromatic to H1′ protons. Panels: (A) the modified strand of the R(61,2) duplex; (B) the unmodified strand of the R(61,2) duplex; (C) the modified strand of the R(61,3) duplex; (D) the unmodified strand of the R(61,3) duplex. The base positions are indicated at the intranucleotide aromatic to sugar H1′ NOE cross-peak.

ras61 oligodeoxynucleotide (Feng & Stone, 1995) and resulted in the overlap of a number of cross-peaks in this region of the spectrum. In the R(61,2) oligodeoxynucleotide, C^1, C^{15}, T^{16}, and C^{20} H6 and G^8 H8 resonated within a small frequency range. T^{13}, T^{14}, and G^{22} H1′ were overlapped, as were A^4, A^{10}, C^{15}, G^{18}, and T^{19} H1′. In the R(61,3) oligodeoxynucleotide, C^1, T^{14}, C^{20}, and C^{21} H6 and G^8 and G^{11} H8 resonated in a small frequency range, and A^4, A^6, T^{13}, T^{14}, C^{15}, and G^{22} H1′ were superimposed, as were A^{10}, G^{11}, and T^{19} H1′.

Exchangeable Protons. The spectra, shown in Figure 2, were similar to those observed for the unmodified *ras61* oligomer (Feng & Stone, 1995). The assignments of the imino resonances were made by sequentially assigning the cross-peaks between imino resonances of neighboring base pairs at 20 °C (Boelens et al., 1985). The non-hydrogen-bonded cytosine amino resonances were assigned from their cross-peaks with the cytosine H5 resonances of the same nucleotide. Hydrogen-bonded cytosine amino resonances were assigned from their strong cross-peaks with the non-

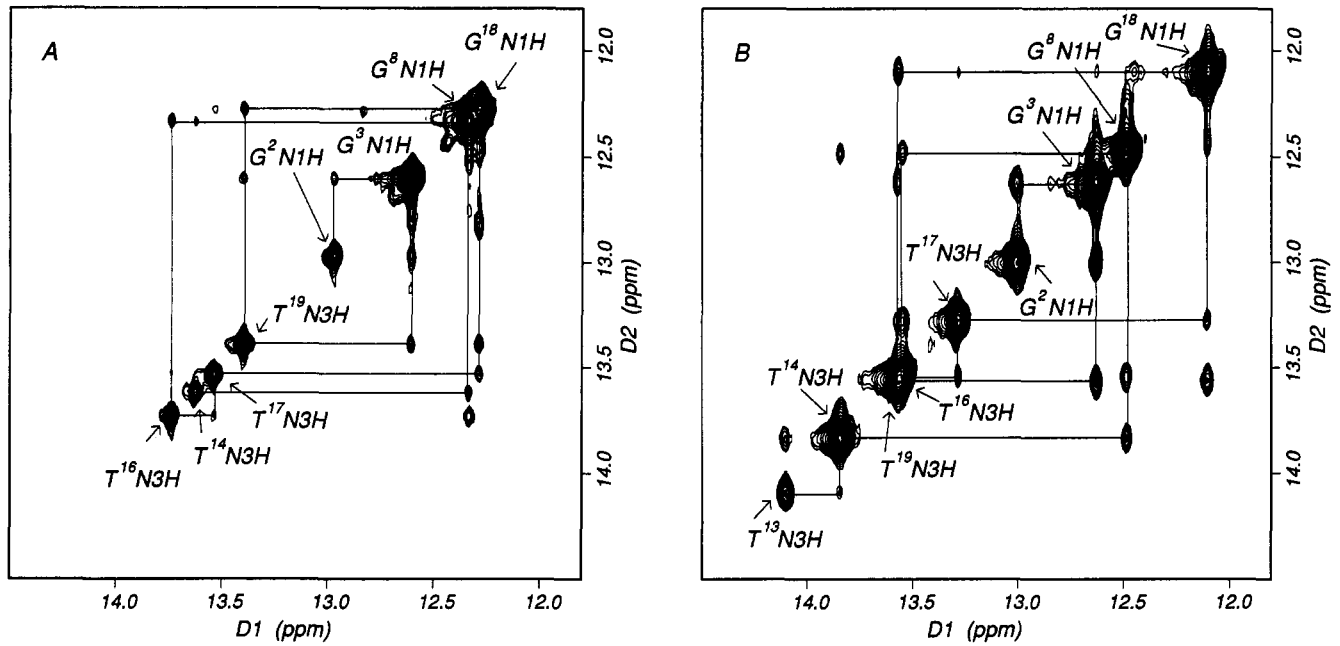

FIGURE 2: Assignments of the imino proton resonances. Panels: (A) the R(61,2) duplex; (B) the R(61,3) duplex.

hydrogen-bonded amino resonances. Cross-peaks between the guanine imino resonances and the hydrogen-bonded amino resonances of the complementary cytosines confirmed the assignments of the guanine imino resonances.

For the R(61,2) duplex, the imino resonance from base pair A^{10}•T^{13} was weak and not observed in Figure 2A. As compared to the unmodified *ras61* oligodeoxynucleotide, a small upfield chemical shift for the imino proton of base pair A^4•T^{19} was observed, on the order of 0.1 ppm. The non-hydrogen-bonded proton of C^5 was not observed. It was believed to be shifted upfield due to the increased shielding of the styrene ring. For the R(61,3) oligodeoxynucleotide, the adenine amino resonance of $^{R\text{-}SO}A^7$ was located at 7.63 ppm. Small upfield chemical shifts were observed for the imino protons of base pairs C^5•G^{18} (0.1 ppm), A^6•T^{17} (0.3 ppm), and $^{R\text{-}SO}A^7$•T^{16} (0.2 ppm). For both modified oligodeoxynucleotides, the imino resonances from the two terminal base pairs C^1•G^{22} and G^{11}•C^{12} were not observed. These underwent rapid exchange with solvent. The exchange-broadened imino resonances from the terminal base pairs were observed in spectra obtained at lower temperatures. The chemical shifts of the exchangeable protons for both oligodeoxynucleotides are listed in Tables 3S and 4S in the supporting information.

Chemical Shift Perturbations of DNA Protons. (a) The R(61,2) Duplex. Several large perturbations were observed, shown in Figure 3. C^5 H6 shifted substantially upfield, from 7.03 ppm in the unmodified oligomer to 6.55 ppm in the modified oligomer. A correspondingly large upfield shift of 1.9 ppm was observed for C^5 H5, which was observed at 3.18 ppm in the adducted oligodeoxynucleotide. $^{R\text{-}SO}A^6$ H8 shifted downfield from 7.98 ppm in the unmodified oligomer to 8.17 ppm in the modified oligomer. C^5 H1′ shifted downfield from 5.22 to 5.33 ppm, $^{R\text{-}SO}A^6$ H1′ shifted from 5.60 to 5.27 ppm (upfield), and A^7 H1′ shifted from 5.71 to 5.96 ppm (downfield). G^8 H1′ shifted from 5.18 to 5.03 ppm (upfield). Examination of the complementary strand also revealed significant changes at and adjacent to the site of adduction. T^{16} H6 shifted from 7.30 to 7.36 ppm (downfield), T^{16} H1′ shifted from 5.84 to 5.97 ppm, and T^{17} H1′ shifted from 5.65 to 5.34 ppm (upfield). T^{17} is the nucleotide opposite the lesion.

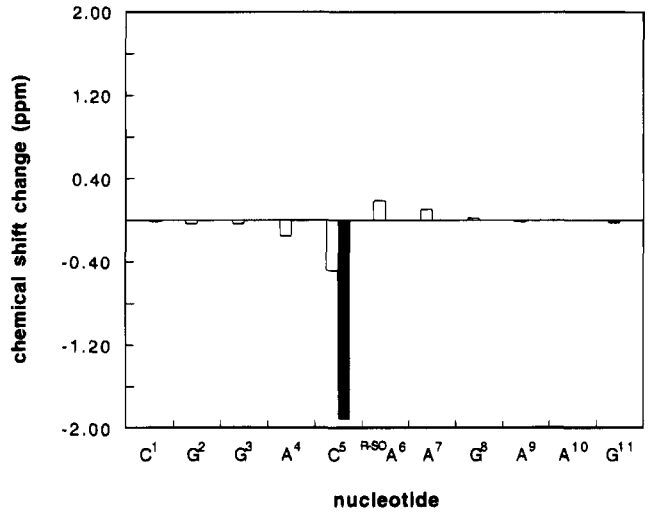

FIGURE 3: Chemical shift changes for the aromatic H8/H6 (open bars) and H5 (solid bars) resonances of the R(61,2) duplex relative to the unmodified *ras61* duplex [$\Delta\delta$ ppm = $\delta_{\text{modified oligomer}} - \delta_{\text{unmodified oligomer}}$ (ppm)].

(b) The R(61,3) Duplex. The localized structural perturbation of the DNA helix was evidenced by the pattern of chemical shift perturbations, which were greatest at and adjacent to the site of adduction and generally decreased toward zero more than two base pairs away from the adduct. The greatest perturbations were observed for the modified strand and were oriented in the 5′-direction from the site of adduction. The largest was an upfield shift from 7.98 to 7.79 ppm, observed for A^6 H8. Smaller upfield perturbations were observed for T^{16} in the complementary strand. In the modified strand, A^6 H1′ and G^8 H1′ exhibited downfield chemical shifts relative to the unmodified duplex.

Styrene Protons. In both the R(61,2) and R(61,3) oligodeoxynucleotides, the benzylic proton, H_b, was identified from TOCSY and NOESY spectra by virtue of a strong cross-peak to the methylenic protons of the CH_2OH group,

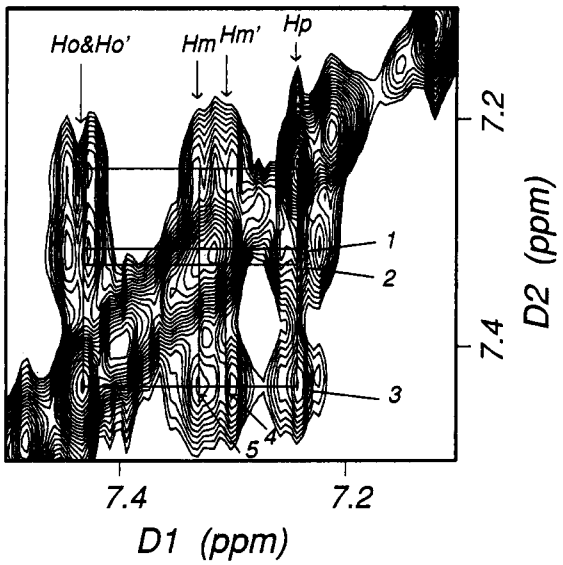

FIGURE 4: Expanded plot of a TOCSY spectrum showing assignments of the styrene phenyl proton resonances in the R(61,3) duplex. Boxes: 1, H_p–$H_{m'}$; 2, H_p–H_m; 3, $H_{o,o'}$–H_p; 4, $H_{o'}$–$H_{m'}$; 5, H_m–H_o.

which exhibited strong coupling. For the R(61,2) adduct, the latter two protons were located at δ 3.61 and 3.64 ppm, while for the R(61,3) adduct, the methylenic protons were observed at δ 3.50 and 3.53 ppm.

In the R(61,2) duplex, the aromatic protons were observed as two signals of area 1:4 at δ 7.41 and 7.37 ppm. The resonance of area 1 at δ 7.41 ppm was assigned to H_m since an NOE was observed between this proton and T^{17} CH_3. The observation of a strong NOE between the H_b proton and the signal of area 4 established that H_o and $H_{o'}$ must be nearly isochronous. It was concluded that the $H_{m'}$ and H_p resonances also were in the signal of area 4 at 7.39 ppm.

In the R(61,3) duplex, the aromatic resonances were observed as five signals between 7.20 and 7.45 ppm. Furthest downfield, and nearly superimposed at 7.43 ppm, were H_o and $H_{o'}$ (Figure 4). These were identified from the NOESY spectrum in which they exhibited a large cross-peak to the benzylic proton. The two meta protons, H_m and $H_{m'}$, were observed as separate resonances at 7.31 and 7.33 ppm. The para proton, H_p, was observed at 7.24 ppm.

Styrene Oxide–DNA NOE Connectivities. (a) The R(61,2) Duplex. With the exception of H_m, individual resonances of the styrene ring were not resolved. NOE connectivities were ascertained by consideration of adduct geometry. These involved major groove DNA protons and were oriented in the 5′-direction from the site of the lesion. The 1.9 ppm ring current shielding of C^5 H5 revealed its proximity to the styrene phenyl moiety. The NOE (Figure 5a) between A^4 H8 and the styrene phenyl protons was assigned to H_p and $H_{m'}$ since in all possible orientations of the styrene ring only H_p and $H_{m'}$ were proximate to A^4 H8. Likewise, inspection of model structures revealed that, in any possible orientation, $H_{o'}$ and $H_{m'}$ would be closest to C^5 H5 and H6, H_p would be further, while H_o and H_m would be sufficiently distant that they would not be likely to show NOEs to C^5 H5 and H6. On the basis of this reasoning, NOEs involving C^5 H5 and H6 were assigned to $H_{o'}$, $H_{m'}$, and H_p. NOEs involving the complementary strand were assigned to H_o and/or H_m. C^5 H6 showed NOEs to $H_{o'}$ and $H_{m'}$ of styrene (Figure 5b), while C^5 H5 showed NOEs to $H_{o'}$, $H_{m'}$, and H_p of styrene (Figure 5f). A long-range NOE was observed between A^4 H2″ and $H_{o'}$ of styrene, as well as $H_{m'}$ of styrene (Figure 5g). On the opposite edge of the styrene ring, H_o exhibited an NOE to T^{16} CH_3 (Figure 5j). T^{16} CH_3 also exhibited NOEs to the methylene protons of the CH_2OH group of styrene (Figure 5k,l). $^{R\text{-}SO}A^6$ H8 showed an NOE to the benzylic proton of styrene, H_b (Figure 5c).

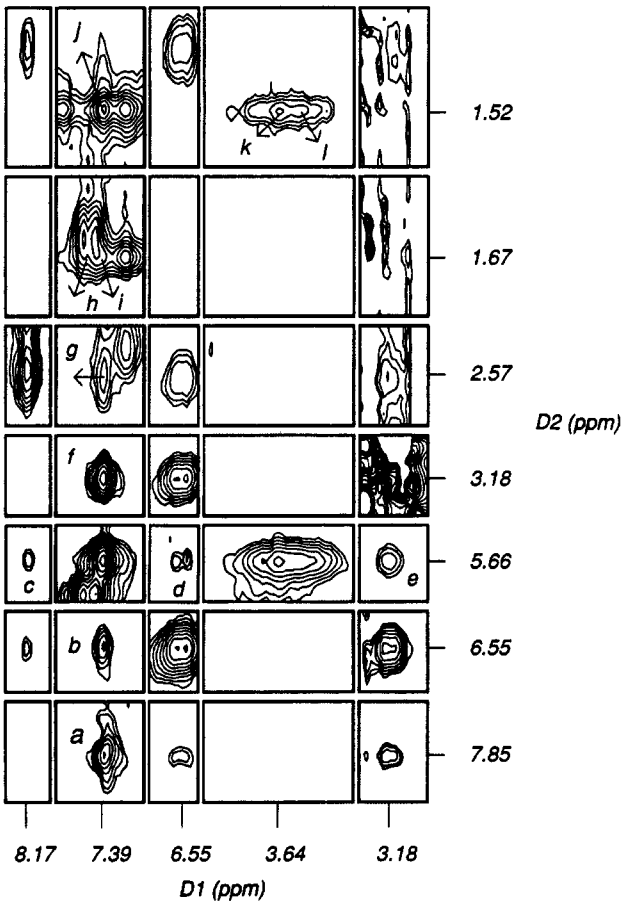

FIGURE 5: NOEs observed between SO and DNA in the R(61,2) duplex: a, A^4 H8 → $H_{m',p}$; b, C^5 H6 → $H_{o',m'}$; c, $^{R\text{-}SO}A^6$ H8 → H_b; d, C^5 H6 → H_b; e, C^5 H5 → H_b; f, C^5 H5 → $H_{o',m',p}$; g, A^4 H2″ → $H_{o',m'}$; h, T^{17} CH_3 → H_m; i, T^{17} CH_3 → H_o; j, T^{16} CH_3 → H_o; k and l, T^{16} CH_3 → $H_{\beta',\beta''}$.

(b) The R(61,3) Duplex. These NOEs also involved major groove protons of the DNA and were oriented in the 5′-direction from the site of the lesion. A^6 H8 showed cross-peaks to $H_{o'}$ and $H_{m'}$ of styrene (Figure 6a,b). C^5, the second nucleotide in the 5′-direction, also exhibited a number of NOEs to the styrenyl ring. C^5 H5 and H6 showed NOEs to $H_{o'}$, $H_{m'}$, and H_p of styrene (Figure 6c-h). On the opposite edge of the styrene ring, H_o and H_m showed cross-strand NOEs to T^{16} CH_3 (Figure 6i,j), the complement to $^{R\text{-}SO}A^7$. In the 3′-direction, NOEs were observed between the benzylic and methylene protons of styrene and DNA protons. $^{R\text{-}SO}A^7$ H8 and $^{R\text{-}SO}A^7$ N6H showed NOEs to the benzylic proton of styrene (Figure 6k,l). T^{14} CH_3, located two base pairs in the 3′-direction, showed NOEs to the methylenic protons of the CH_2OH group (Figure 6p). Cross-strand NOEs were observed between C^{15} NH_2 and the methylene protons of the CH_2OH group (Figure 6m,o). A weak NOE was observed between the benzylic proton of the SO and the H2′ deoxyribose proton of A^6.

(c) Spin Diffusion. At 250 ms mixing time, both first-order and higher order NOEs were observed in the R(61,2)

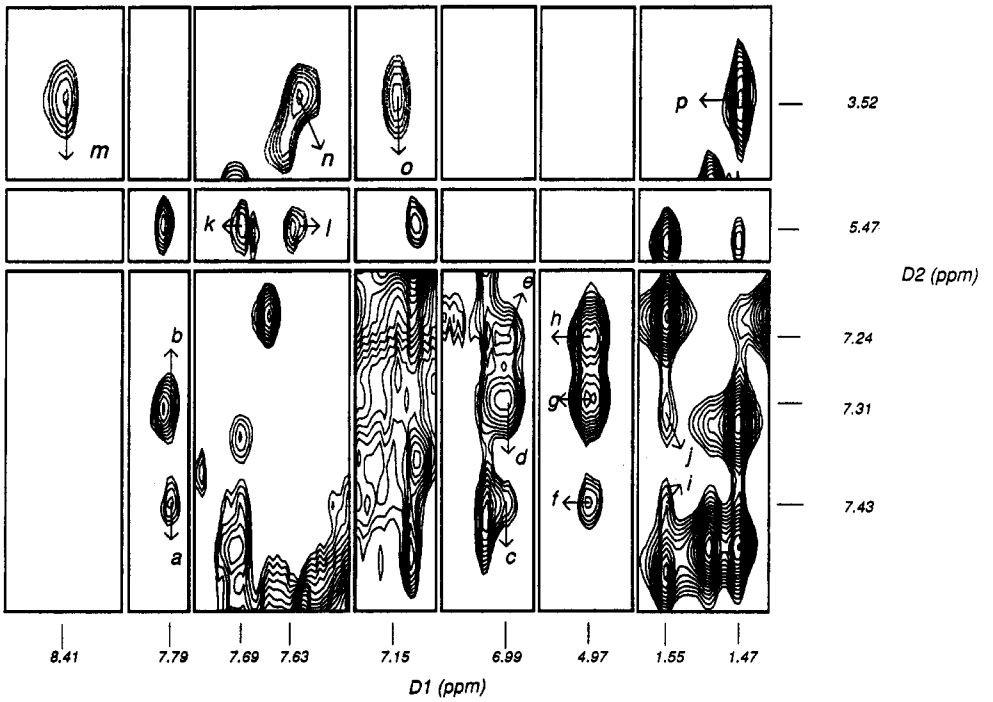

FIGURE 6: NOEs observed between SO and DNA in the R(61,3) duplex: a, A^6 H8−$H_{o'}$; b, A^6 H8−$H_{m'}$; c, C^5 H6−$H_{o'}$; d, C^5 H6−$H_{m'}$; e, C^5 H6−H_p; f, C^5 H5−$H_{o'}$; g, C^5 H5−$H_{m'}$; h, C^5 H5−H_p; i, T^{16} CH_3−H_o; j, T^{16} CH_3−H_m; k, $^{R\text{-}SO}A^7$ H8−H_b; l, $^{R\text{-}SO}A^7$ N6H−H_b; m, CH_2OH−C^{15} N4H (hydrogen-bonded); n, $^{R\text{-}SO}A^7$ N6H−CH_2OH; o, C^{15} N4H (non-hydrogen-bonded)−CH_2OH; p, CH_2OH−T^{14} CH_3.

and R(61,3) spectra, due to the strongly coupled styrene ring protons. NOEs observed between C^5 H5 and H6 and H_b of styrene in the R(61,2) oligodeoxynucleotide (Figure 5d,e) were believed to be due to spin diffusion, via $H_{o'}$. Likewise, the NOE observed between C^5 H6 and $H_{o'}$ of styrene in the R(61,3) adduct was believed to be due to spin diffusion, via $H_{m'}$, as was the NOE between C^5 H5 and $H_{o'}$ (Figure 6c,f). Additional NOEs were observed between the H2′ and H2″ protons of C^5 and $H_{m'}$ and $H_{o'}$ of SO in the R(61,3) adduct. The NOEs to the H2″ protons were undoubtedly a result of strong spin diffusion between the geminally coupled H2′ and H2″ protons. These NOEs became weaker at the shorter mixing time of 100 ms.

Molecular Dynamics. Structural refinement of the R(61,2) duplex was complicated by spectral overlap of the styrene resonances. Two approaches, both of which involved inspection of molecular models to predict the magnitudes of expected NOEs between styrene aromatic protons and DNA, were used. In the first, overlapped cross-peaks between styrene aromatic protons and DNA protons in the modified strand at δ 7.39 ppm were not included in the NOE intensities used by MARDIGRAS. They were assumed to include both first- and second-order contributions from $H_{o'}$, $H_{m'}$, and H_p. Distances between the styrene and DNA protons obtained from inspection of model structures were assigned as strong, medium, and weak distance restraints in MD calculations, with ranges of 1.8−2.5, 1.8−3.5, and 1.8−5 Å, respectively. The second method assumed that $H_{o'}$ of styrene provided the major source of dipolar coupling to the overlapped NOE cross-peaks with C^5 H5 and H6, C^5 H2″, and A^4 H3′. The intensity of cross-peaks between C^5 H5 and H6 and the overlapped styrene aromatic resonances at δ 7.39 ppm was assigned to contributions primarily from $H_{o'}$. These intensities were included in MARDIGRAS, and distances calculated for $H_{o'}$ were included as restraints in the MD calculations.

Table 1: DNA-Styrene Distance Restraints Derived from NOE Data Using MARDIGRAS and Measured from the Refined Structure for the R(61,2) and R(61,3) Adducts

DNA proton	styrene proton	distance calcd from MARDIGRAS (upper and lower bounds) (Å)	av distance measured from 10 refined structures (Å)
		(a) R(61,2) Adduct	
A^4 H2″	$H_{o'}$	2.1−3.5	3.61 ± 0.03
A^4 H3′	$H_{o'}$	4.6−5.8	5.11 ± 0.16
C^5 H5	$H_{o'}$	2.4−2.8	2.90 ± 0.09
C^5 H5	H_b	3.9−4.3	3.74 ± 0.03
C^5 H6	$H_{o'}$	3.6−4.3	3.87 ± 0.25
A^6 H8	H_b	3.7−4.1	3.93 ± 0.02
T^{16} CH_3	$H_{\beta''}$	4.1−4.7	4.62 ± 0.25
T^{16} CH_3	H_o	3.3−4.5	4.59 ± 0.41
		(b) R(61,3) Adduct	
C^5 H5	$H_{o'}$	6.0−7.0	5.94 ± 0.02
C^5 H5	$H_{m'}$	3.2−3.6	3.78 ± 0.01
C^5 H5	H_p	3.2−3.6	3.08 ± 0.02
C^5 H6	$H_{m'}$	3.4−3.8	3.31 ± 0.02
C^5 H6	H_p	3.5−3.9	4.02 ± 0.01
A^6 H8	$H_{o'}$	2.4−2.8	2.96 ± 0.03
A^6 H8	$H_{m'}$	3.0−4.1	3.63 ± 0.09
T^{14} CH_3	$H_{\beta'}$	5.6−6.3	5.22 ± 0.49
T^{14} CH_3	$H_{\beta''}$	5.2−5.9	4.89 ± 0.56

Both methods yielded similar refined structures for the R(61,2) adduct. The structures shown in Figure 7A−C were obtained using the second method. The final restraints consisted of 260 of the original 286 distances. Including empirical restraints, a total of 310 restraints were used, of which 8 were distances between styrene and DNA protons and 50 were base-pairing restraints. Four of the 8 styrene−DNA restraints involved $H_{o'}$ of the styrene ring (Table 1a). An average of 22 intranucleotide, internucleotide, and empirical distances was obtained for each base pair, excluding the terminal base pairs, collected in Table 5S in the supporting information. No base-step restraints were used.

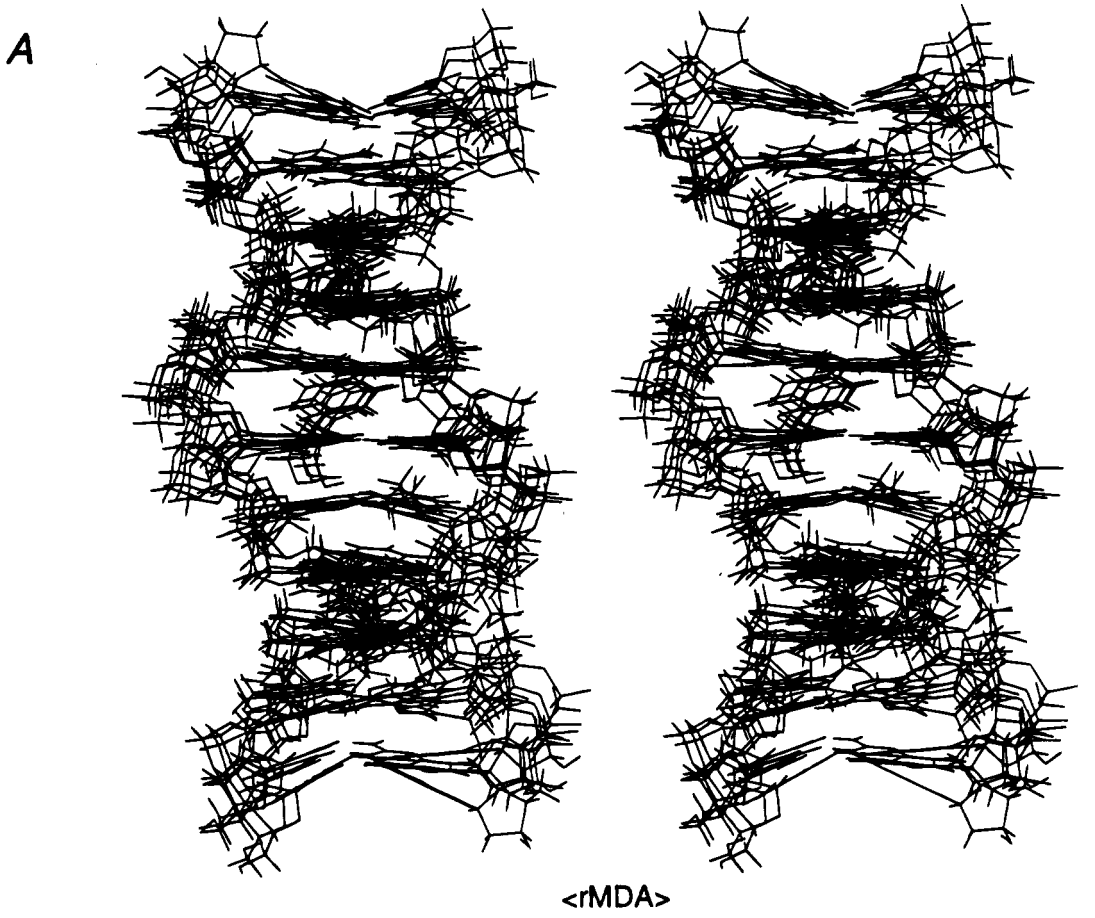
A
<rMDA>

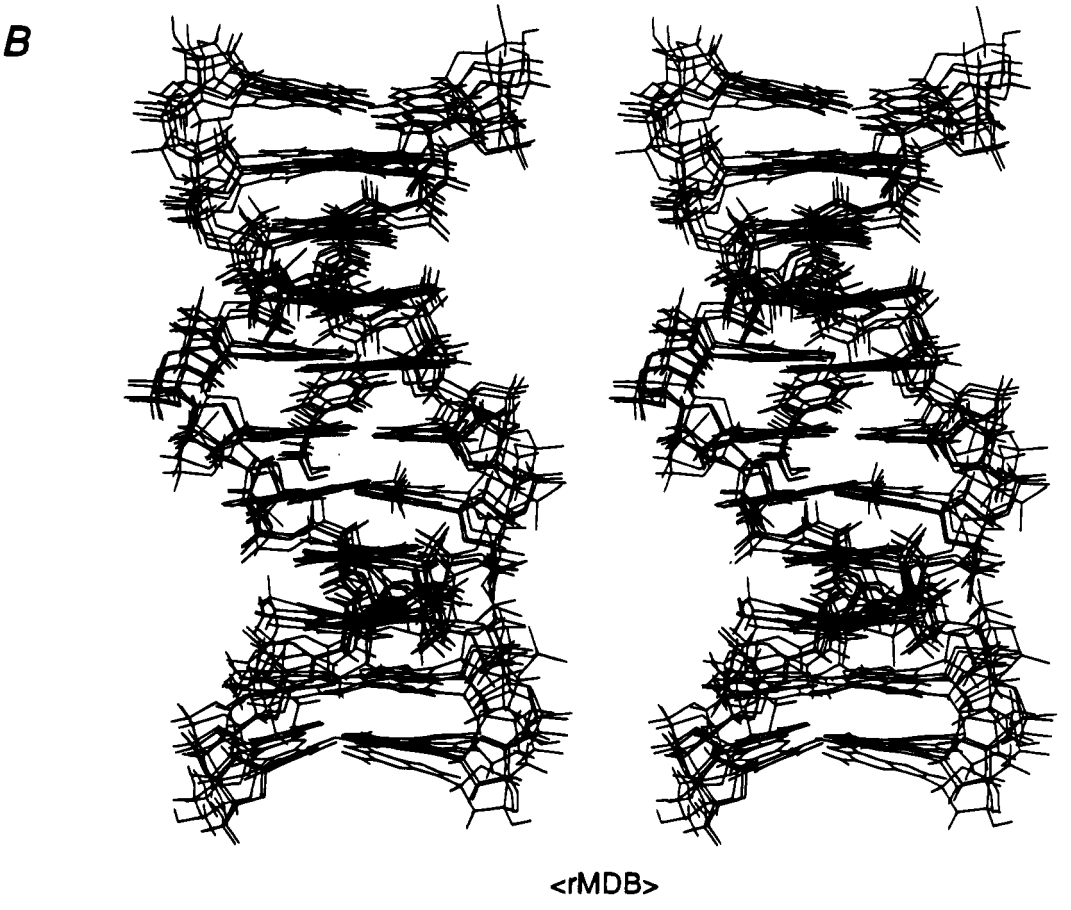
B
<rMDB>

C

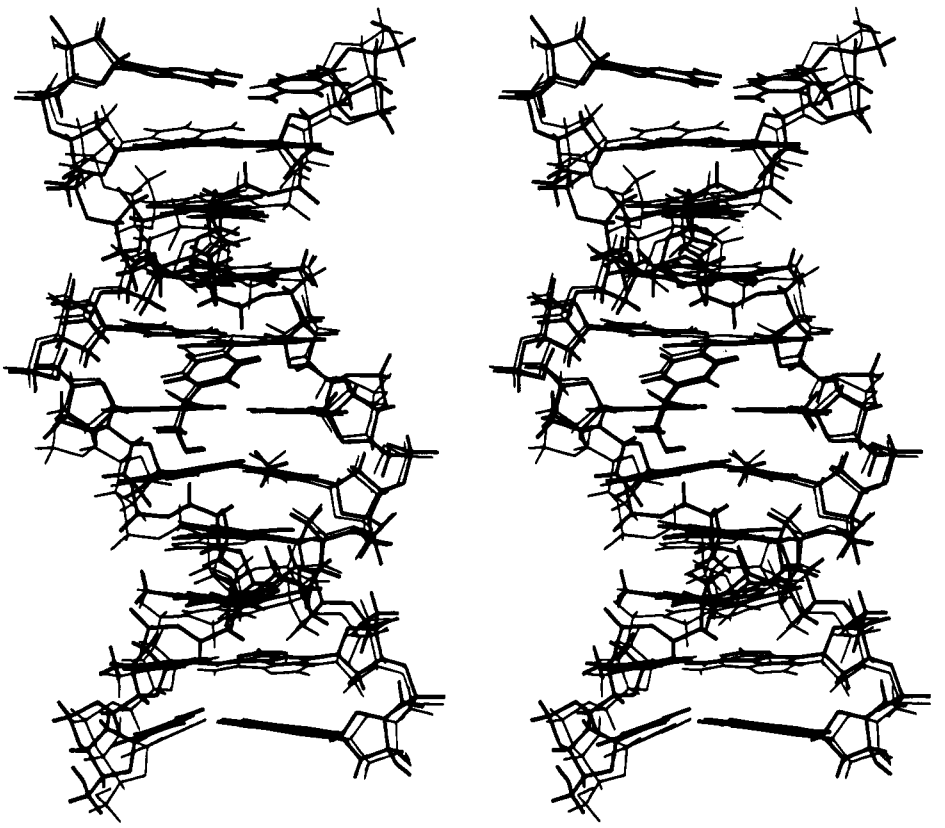

rMDA vs. rMDB

D

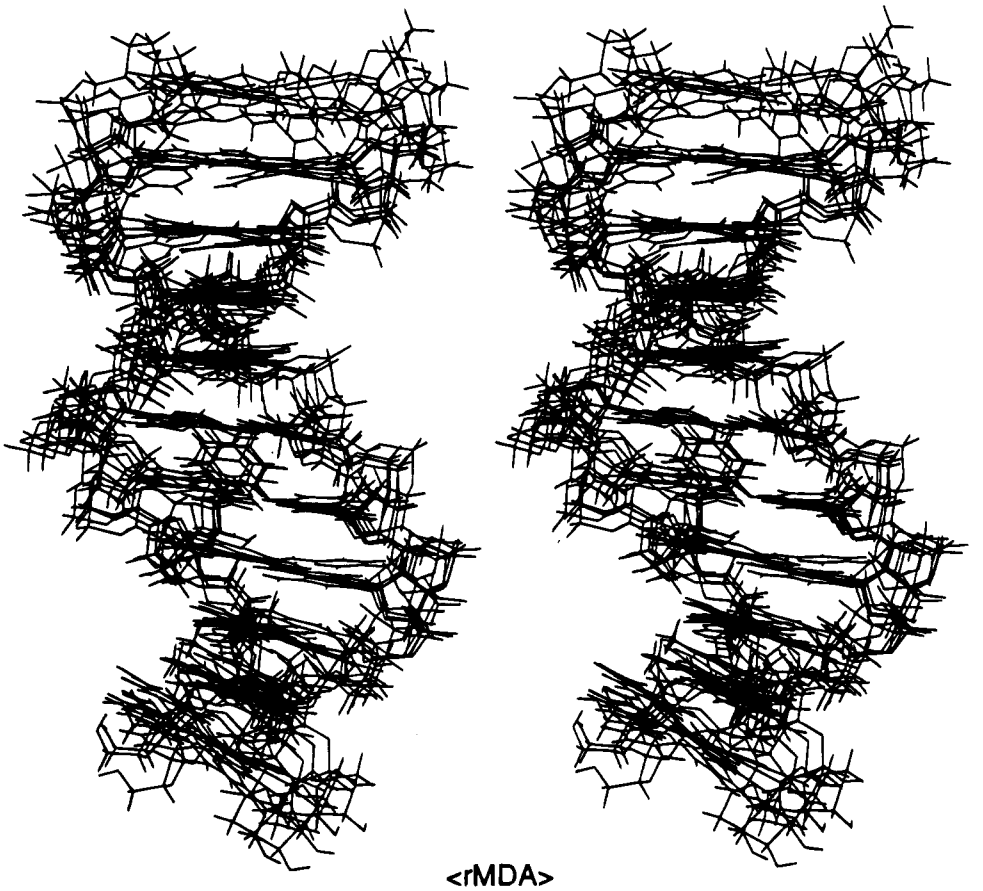

<rMDA>

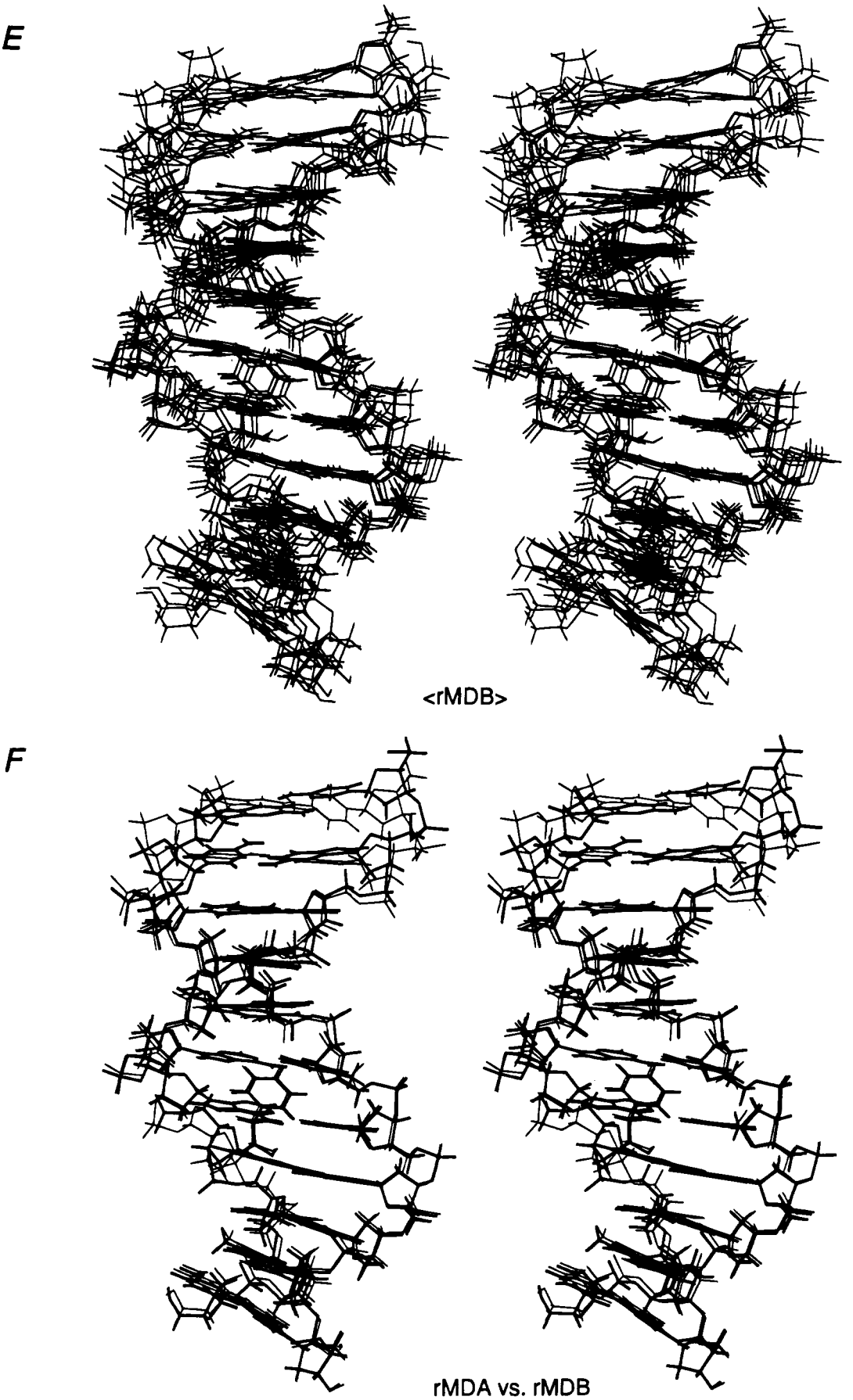

FIGURE 7: (A) Superposition of MD structures based upon the IniA starting structure for the R(61,2) duplex. (B) Superposition of MD structures based upon the IniB starting structure. (C) Superposition of the rMDA and rMDB (bold) structures. (D) Superposition of MD structures based upon the IniA starting structure for the R(61,3) duplex. (E) Superposition of MD structures based upon the IniB starting structure. (F) Superposition of the rMDA and rMDB (bold) structures. In each instance, five randomly seeded calculations were performed.

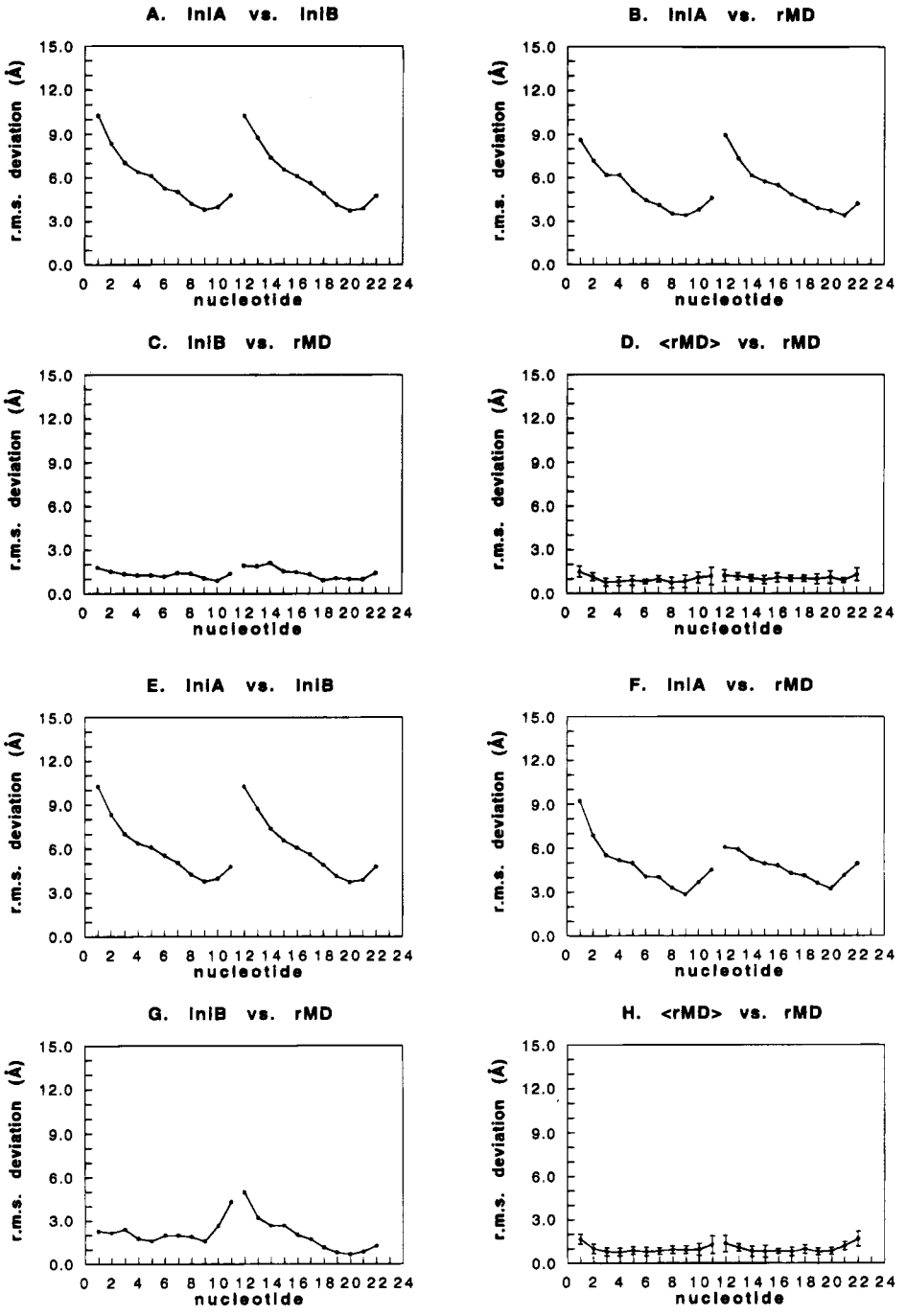

FIGURE 8: Per residue rmsd comparisons between the initial structures and the final structures. R(61,2) duplex: (A) comparison of IniA vs IniB; (B) comparison of IniA vs rMD; (C) comparison of IniB vs rMD; (D) comparison of ⟨rMD⟩ vs rMD of each of the final structures with the energy-minimized average of the 10. R(61,3) duplex: (E) comparison of IniA vs IniB; (F) comparison of IniA vs rMD; (G) comparison of IniB vs rMD; (H) comparison of ⟨rMD⟩ vs rMD of each of the final structures with the energy-minimized average of the 10. The error bars represent the standard deviation observed at each nucleotide. The slopes of the data in this figure reflect the choice in reference frame in calculating the rms deviations.

For the R(61,3) duplex, the final restraints consisted of 230 of the original 273 distances calculated by MARDIGRAS. Including empirical restraints, a total of 289 restraints were used, of which 50 were base-pairing restraints, and 9 were base-step restraints, between nucleotides C^1 and G^2, G^2 and G^3, A^9 and A^{10}, A^{10} and G^{11}, C^{12} and T^{13}, T^{13} and T^{14}, C^{19} and C^{20}, C^{20} and C^{21}, and C^{21} and G^{22}. A total of 9 styrene−DNA distance restraints derived from MARDIGRAS were included to derive the structures shown in Figure 7D−F and tabulated in Table 1b. An average of 21 intranucleotide, internucleotide, and empirical distances were obtained for each base pair, excluding terminal base pairs, collected in Table 6S in the supporting information. The complete set of experimental and empirical restraints for both the R(61,2) and R(61,3) oligodeoxynucleotides are collected in Tables 7S and 8S in the supporting information.

For both the R(61,2) and R(61,3) duplexes, structures calculated from IniA and IniB converged to similar structures, which resembled B-DNA. The final structures for the R(61,2) oligodeoxynucleotide are shown in Figure 7A,B. Figure 7C shows the superposition of the average structures emergent from either IniA or IniB. The final structures for the R(61,3) oligodeoxynucleotide are shown in Figure 7D,E. Figure 7F shows the superposition of the average structures

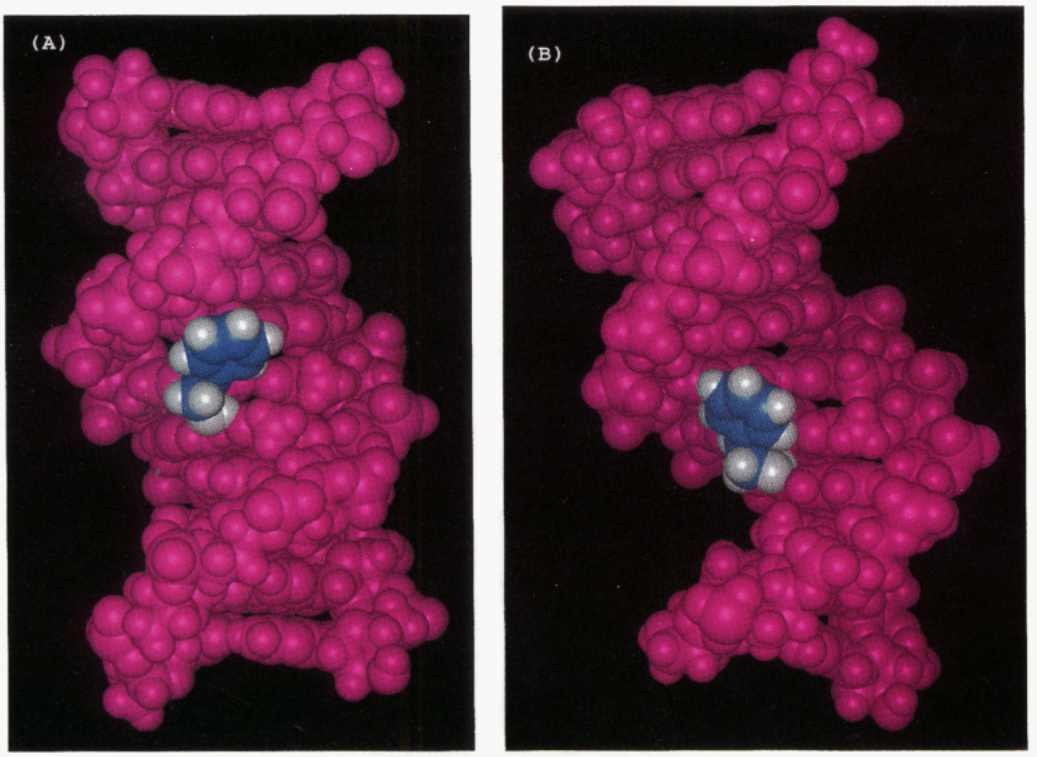

FIGURE 9: CPK representations of the final MD structures: (A) the R(61,2) duplex; (B) the R(61,3) duplex. SO is shown in blue. Protons on SO are shown in white. These model structures are based upon averaging the coordinates from 10 MD calculations (see text).

emergent from either IniA or IniB.

The emergent structures were monitored as to precision by pairwise measurements of rms deviations, shown in Figure 8A−D for the R(61,2) oligodeoxynucleotide and Figure 8E−H for the R(61,3) oligodeoxynucleotide. Figure 8A,E confirms the large difference between the starting structures IniA and IniB, on the order of 6 Å rmsd. Figures 8B,F and 8C,G reveal that the structures emergent from the calculations were closer to IniB than to IniA. The MD calculations resulted in the convergence of the IniA structures toward B-like final structures. Figure 8D,H shows pairwise comparison of emergent structures from the MD calculations. In both the R(61,2) and R(61,3) duplexes, the structural refinement procedure defined one family of structures with good precision. In each case, the 10 MD structures were averaged and potential energy minimized to obtain the final rMD structures shown in Figure 9. The average rmsd for the R(61,2) duplex was found to be 1.3 Å, with the maximum rmsd (between the two most differing structures) measured as 1.7 Å. The average rmsd for the R(61,3) duplex was 1.2 Å, with the maximum measured as 1.6 Å.

Relaxation Matrix Calculations. Table 2 shows *R*-factors calculated for the starting structures and the rMD structures, calculated at three values of NOE mixing time using CORMA (Keepers & James, 1984). For both the R(61,2) and R(61,3) oligodeoxynucleotides, *R*-factors decreased when the starting structures IniA and IniB were compared to the rMDA and rMDB structures which emerged from the calculations. Consistent results were obtained at each of the three mixing times. The best values were observed for the 250 ms data, which reflected the improved sensitivity of the longer mixing time data. As compared to the starting structures, which exhibited different *R*-factors, the values calculated for the emergent rMDA and rMDB structures for the R(61,2) duplex were 7.5×10^{-2} at 250 ms. The corresponding values for the R(61,3) duplex were 6.8×10^{-2} at 250 ms. The RMA calculations suggested that the refined family of structures was in reasonable agreement with the available NOE-based restraints

Table 2: Comparison of Sixth Root Residual Indices R_1^x for Starting Models and Resulting MD Structures as a Function of NOE Mixing Time for the R(61,2) and R(61,3) Duplexes[a]

	(a) R(61,2) Duplex R_1^x ($\times 10^{-2}$)		
structure	$t_m = 150$ ms	$t_m = 200$ ms	$t_m = 250$ ms
IniA	16.6	15.7	15.1
IniB	9.24	9.30	9.27
rMDA	7.60	7.50	7.46
rMDB	7.71	7.70	7.66
rMD_{final}	7.45	7.39	7.52
	(b) R(61,3) Duplex R_1^x ($\times 10^{-2}$)		
structure	$t_m = 100$ ms	$t_m = 150$ ms	$t_m = 250$ ms
IniA	17	15	14
IniB	11	10	10
rMDA	7.9	7.3	6.8
rMDB	7.9	7.3	6.8
rMD_{final}	7.6	7.1	6.7

[a] Only the inner nine base pairs were used in the calculations to exclude end effects. [b] $R_1^x = \sum|(a_o)_i^{1/6} - (a_c)_i^{1/6}|/\sum|(a_o)_i^{1/6}|$, where a_o and a_c are the intensities of observed (non-zero) and calculated NOE cross-peaks. IniA, starting energy-minimized A-DNA; IniB, starting energy-minimized B-DNA; rMDA, average of five rMD structures starting from IniA; rMDB, average of five MD structures starting from IniB; rMD_{final}, average of 10 MD structures starting from IniA and IniB.

DISCUSSION

Mutagenesis at codon 61 in *n-ras* and related protooncogenes leads to oncogene activation. The detailed structural refinement of (*R*)-α-(N^6-adenyl)styrene oxide adducts ex-

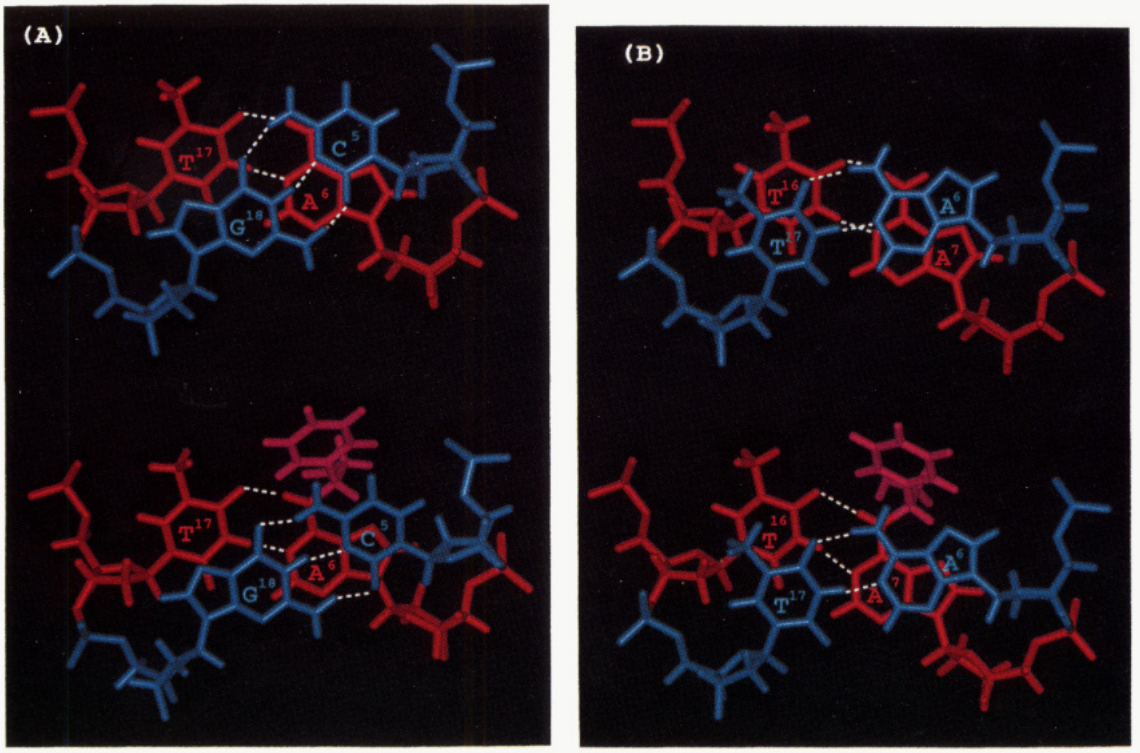

FIGURE 10: (A) Comparison of stacking patterns of the C^5·G^{18} base pair with (top panel) A^6·T^{17} in the unmodified *ras61* oligodeoxynucleotide and (bottom panel) $^{R-SO}A^6$·T^{17} in the R(61,2) oligodeoxynucleotide. (B) Comparison of stacking patterns of the A^6·T^{17} base pair with (top panel) A^7·T^{16} in the unmodified *ras61* oligodeoxynucleotide and (bottom panel) $^{R-SO}A^7$·T^{16} in the R(61,3) oligodeoxynucleotide.

amine the hypothesis that DNA sequence modulates the conformation of isomeric (*R*)-α-(*N*^{6}-adenyl)styrene oxide adducts within the *ras61* oligodeoxynucleotide. Comparison of the R(61,2) adduct with the R(61,3) adduct demonstrates small, but discernible sequence-specific alterations in adduct structure within the *ras61* oligodeoxynucleotide, a context in which adduct-induced mutations are associated with carcinogenesis. These may correlate with differences in DNA replication for the R(61,2) and R(61,3) adducts (Latham et al., 1993, 1995; Latham & Lloyd, 1994).

Oligodeoxynucleotide Conformation. The major groove location of the styrenyl moieties in the R(61,2) and R(61,3) adducts suggested that they might be accommodated with minimal perturbation of the DNA duplex. The R(61,2) and R(61,3) SO adducts adopted conformations in the B-family, which have modest structural perturbations at and adjacent to the lesion site. Evidence that the right-handed helix is B-like for both the R(61,2) and R(61,3) adducts was obtained from the intensities of the NOEs between the H8/H6 and the H2′ and H2″ protons of the same residue and from their estimated distances (Reid, 1987). The greater NOE intensities of the cross-peaks between the H8/H6 of the guanine and cytosine residues and the H2′ and H2″ of the same residue as compared to the intensities of the cross-peaks between the H8/H6 and the H1′ protons of the attached deoxyribose moieties suggested that these residues adopt the *anti* conformation about the glycosidic bond (Patel et al., 1982). Further support for a right-handed helix was reflected in the cross-peaks observed between purine H8 and pyrimidine H5 and CH_3 protons on adjacent bases in the direction of purine (5′−3′) pyrimidine but not in the direction pyrimidine (5′−3′) purine (Patel et al., 1987).

Structural refinement confirmed that these two modified duplexes remained B-like in conformation. Figure 10 details calculated stacking patterns at the SO lesion sites. For both lesions the SO adduct occupied the major groove of the DNA and was oriented in the 5′-direction from the sites of attachment at $^{R-SO}A^6$ or $^{R-SO}A^7$. Base-pairing interactions remained intact at the sites of the lesions, consistent with the NMR data for the imino protons (Figure 2). In each instance, the styrenyl protons interacted primarily with the modified strand. The NOE data were corroborated by chemical shift perturbations adjacent to the sites of adduction. Protons in the major groove and located on the 5′ side of the adduct in the modified strand underwent increased shielding, interpreted to arise from the proximity of the styrene ring. This effect was particularly pronounced for C^5 H5 in the R(61,2) adduct, which shifted upfield by approximately 2 ppm (Figure 3). C^5 H6 in this adduct was likewise shifted, approximately 0.5 ppm upfield. The 5′-neighbor A^6 was located near the styrene ring in the R(61,3) adduct, resulting in an upfield shift for A^6 H8. An interesting comparison was made between the R(61,3) and R(61,2) adducts. Figure 10 suggests that the smaller upfield shift observed for A^6 H8 in the R(61,3) oligodeoxynucleotide resulted because this proton was less exposed in the major groove and experienced less shielding from the styrene aromatic ring. A calculated decreased twist of the helix at the adduct site for the R(61,3) adduct allowed the styrene to be positioned in the major groove without steric crowding from the 5′-neighbor A^6·T^{17} base-pair.

The NMR data allowed the styrene rings to be located with confidence, but their precise orientations were not well defined. The overlap of the aromatic resonances, particularly for the R(61,2) adduct, prevented complete assignments of the styrene protons and hindered accurate volume integration. Parts a and b of Table 1, which compare average styrene−DNA distances measured from 10 refined structures with

distances calculated by MARDIGRAS, illustrate this. For the R(61,2) adduct, the refined structures and the NMR data were in qualitative agreement. Four of eight average styrene−DNA distances measured from the refined structures agreed with the distances predicted from NOE data. Three of the remaining four measured average distances were within 0.1 Å of the MARDIGRAS-calculated structures. A less satisfactory result was obtained for the R(61,3) adduct, for which only one average distance measured from 10 refined structures was within the distance restraints calculated by MARDIGRAS, although four additional average distances were within 0.1 Å of the NOE-predicted distances. The refined structure of the R(61,2) adduct did not explain chemical shift changes for $^{R\text{-}SO}A^6$ H1′ and A^7 H1′, which shifted upfield 0.3 ppm and downfield 0.3 ppm, respectively. These differences were suspected to result from alterations in base stacking orientation of the C^5•G^{18} and $^{R\text{-}SO}A^6$•T^{17} base pairs which would bring the respective H1′ protons either under greater or lesser influence of ring current interactions.

Dynamics of the Styrene Moiety. The resolution of the styrene ring H_m and $H_{m'}$ resonances in both the R(61,2) and R(61,3) oligomers revealed that ring flips of the styrene moiety were slow on the NMR time scale. The symmetric styrene ring protons became nonequivalent in the asymmetric DNA environment, analogous to phenylalanine and tyrosine rings within the interior of globular proteins (Wuthrich & Wagner, 1978). The geometry of the styrene CH_2OH moiety was not well defined in the calculated R(61,2) and R(61,3) structures. The MD calculations suggested the potential for hydrogen bond formation in the R(61,2) adduct, between the hydroxyl group of SO and T^{16} O4, of the neighboring base pair in the 3′-direction. For the R(61,3) adduct, the calculations suggested that the hydroxyl group provided a potential hydrogen bond to G^8 O6, the nucleotide 3′ to the site of the lesion. These were not observed in the spectra, perhaps because the rate of exchange with solvent prevented their observation. Also of interest was the potential for rotation of either the R(61,2) or R(61,3) adducts about the adenyl N6−C_α bonds, which would interchange the orientation of the styrene ring within the major groove between the 3′- and 5′-directions. This was not observed in either instance.

Sequence Dependence. When the R(61,2) adduct was compared to the R(61,3) adduct, similarities were observed. In both, the R-SO moiety was oriented in the 5′-direction from the adducted adenosine, either $^{R\text{-}SO}A^6$ or $^{R\text{-}SO}A^7$. Also, in both adducts, the R-SO moiety was accommodated in the major groove, without gross conformational distortion of the DNA duplex. The calculations did suggest differences between these adducts. In the preferred orientation calculated for the R(61,2) adduct, the styrene ring was oriented edgewise in the major groove such that it was approximately orthogonal to the edge of the C^5 pyrimidine ring. The preferred orientation calculated for the R(61,3) duplex had the styrene ring oriented on the floor of the major groove approximately orthogonal to the major groove edge of the two base pairs, A^6•T^{17} and $^{R\text{-}SO}A^7$•T^{16}. The refined structures suggested why this might be the case. For the R(61,2) adduct the 5′-neighbor nucleotide was cytosine, whereas for the R(61,3) adduct, the 5′-neighbor was adenine. The purine ring did not protrude into the major groove of the DNA to the extent that a pyrimidine ring did, and the R(61,2) adduct appeared to be more sterically hindered than did the R(61,3) adduct.

These structures can be compared to the bulkier PAH (−)-10(*R*)-benzo[*a*]pyrene adenyl N6 (Schurter et al., 1995) and (−)-*trans-anti*-benzo[*c*]phenanthrene adenyl N6 adducts (Cosman et al., 1995). In each of these, the planar aromatic ring system is intercalated from the major groove. A benzo[*a*]pyrene adenyl N6 adduct currently under refinement in our laboratory also is intercalated. Thus, the R(61,2) and R(61,3) SO lesions differ from the bulkier PAH adducts at adenine N6, in that they do not exhibit a tendency toward intercalation. Perhaps this is because styrene oxide can rotate about the C_α−phenyl bond, in contrast to the PAH adducts which are covalently constrained.

Comparison to Replication Studies. Factors likely to contribute to the fate of SO adducts *in vivo* include repair competence, sequence context (Zarbl et al., 1985; Topal et al., 1986; Glickman et al., 1987; Randall et al., 1987; Topal, 1988; Burnouf et al., 1989; Rodriguez & Loechler, 1993; Shibutani & Grollman, 1993; Wilson et al., 1993; Latham & Lloyd, 1994), and the ability of replication complexes to bypass the damage. Primer extension studies using bacterial and eukaryotic polymerases revealed that templates bearing R(61,2) and R(61,3) adducts were replicated differently (Latham et al., 1995). Studies using HIV-1 reverse transcriptase (Latham & Lloyd, 1994), Klenow fragment, Sequenase 2.0, T4 polymerase holoenzyme, and human polymerases α and β revealed two notable features associated with the replication of the R(61,2) adduct: (1) slow kinetics of bypass synthesis and (2) significant variations in the efficiency of translesion synthesis depending on the choice of polymerase (Latham et al., 1995). In contrast, these polymerases readily extended the R(61,3)-adducted templates. For the R(61,2) adduct, polymerization was generally terminated either opposite or one base 3′ to the adduct, although primer extension mediated by HIV-1 reverse transcriptase resulted in stop sites three bases after translesion synthesis but before reaching the end of the template (Latham & Lloyd, 1994). When replication was restricted to single catalytic cycles, the R(61,2) lesion presented a strong block to all polymerases examined, limiting the accumulation of fully extended primers. Although bypass was facilitated in most cases when excess polymerase was used to drive the reactions, significantly, polymerase β, an enzyme implicated in gap-filling repair synthesis, was still unable to synthesize full-length products from R(61,2)-adducted templates (Latham et al., 1995). For the R(61,2) adduct, differing replication results using a variety of polymerases seemed to reflect structural differences in the respective primer-template replication complexes and supported the notion that lesion bypass is polymerase specific (Shibutani et al., 1991; Comess et al., 1992; Shibutani, 1993; Basu et al., 1993; Belguise-Valladier et al., 1994). The poor kinetics of lesion bypass could be expected to enhance the possibility of misincorporation opposite the damage site. To examine this possibility, adduct-directed mutagenesis studies utilizing this R(61,2) SO adduct are in progress.[4]

The differences between the equilibrium conformations of these two adducts, involving orientation of the phenyl ring in the major groove, seem small. How might they account for differences in *in vitro* replication for the R(61,2) vs the R(61,3) adduct (Latham et al., 1993, Latham & Lloyd, 1994)? One possibility is that equilibrium adduct conforma-

[4] Gary J. Latham and R. Stephen Lloyd, personal communication.

tions as obtained in these studies may not be representative of structural differences during replication or repair (Randall et al., 1987; Singer et al., 1989; Voigt & Topal, 1990; Rodriguez & Loechler, 1993). Alternatively, small structural differences between these two adducts perhaps lead to significant alteration of nucleotide insertion and strand extension kinetics opposite the R(61,2) adduct as compared to the R(61,3) adduct. Support for this hypothesis comes from evidence that correct nucleotide insertion during replication is dependent upon attainment of the correct geometry of the incoming nucleotide (Goodman et al., 1993). The present studies suggest greater structural perturbation in the case of the R(61,2) adduct, due to major groove steric clashes between the styrenyl ring and the 5′-neighbor cytosine, which are not as severe in the case of the R(61,3) adduct which has a 5′-neighbor adenine (Figure 9). We speculate that these cause adduct-induced changes in primer-template geometry and lowered efficiency of the replication complex, resulting in stalling at the R(61,2) lesion.

Arylamine Adducts in the ras61 Coding Sequence. Adducts of *N*-2-aminofluorene and aminobiphyenyl were examined in the murine *c-Ha-ras* sequence (Cho et al., 1992, 1994), while the *N*-2-aminofluorene adduct was examined in the model human *c-H-ras*1 sequence (Eckel & Krugh, 1994a,b). The *c-ha-ras61* sequence differed from the *n-ras* sequence by substituting adenine for cytosine at the wobble position of codon 59 and by substituting thymine for adenine at the wobble position of codon 60. The model *c-H-ras1* sequence, designed to control the regioselectivity of arylamine adduction, substituted guanine for adenine at the wobble position of codon 61, as compared to the *n-ras* sequence. The conformations of the adenine N6 SO adducts differed from the arylamine guanine C8 lesions. For the arylamines, conformational exchange was observed between external orientations with minimal perturbation of the double helix and internal orientations with base displacement to accommodate the intercalated arylamine. The equilibrium distributions between conformers in the *c-Ha-ras* sequence were dependent upon adduct structure. The *N*-2-aminofluorene adduct exhibited a greater tendency to form the minor (intercalated) structure (Cho et al., 1992, 1994). The ability of the *N*-2-aminofluorene adduct to interchange conformation on the same time scale as DNA replication was described as a "mutagenic switch" (Eckel & Krugh, 1994a,b), in which each conformation might generate a separate mutagenic outcome.

Summary. Two isomeric (*R*)-α-(*N*^{6}-adenyl)styrene oxide adducts were readily accommodated within the major groove of DNA. Both were oriented such that the styrenyl moiety faced the 5′-direction from the site of adduction. The conformational differences between these two adducts were small and involved differences in the energy-minimized conformations of the styrenyl moieties, presumably due to nearest neighbor effects in the 5′-direction.

ACKNOWLEDGMENT

Drs. James G. Moe and Irene S. Zegar, Mr. Jason P. Weisenseel, and Mr. Markus Voehler assisted with NMR spectroscopy and structural refinement. Mr. Gary J. Latham and Professor R. Stephen Lloyd (The University of Texas Medical Branch, Galveston) provided helpful discussions.

SUPPORTING INFORMATION AVAILABLE

Tables S1−S8, which detail the ^{1}H NMR chemical shift assignments, the distributions of NOE restraints, and the experimental distances and classes of restraints for the R(61,2) and R(61,3) oligodeoxynucleotides, and Figure S1, which shows force field parametrization values used for styrene oxide (18 pages). Ordering information is given on any current masthead page.

REFERENCES

Barbacid, M. (1987) *Annu. Rev. Biochem. 56*, 779−827.
Basu, A. K., Hanrahan, C. J., Malia, S. A., Kumar, S., Bizanek, R., & Tomasz, M. (1993) *Biochemistry 32*, 4708−4718.
Bax, A., Sklenar, V., & Clore, G. M. (1987) *J. Am. Chem. Soc. 109*, 6511−6513.
Belguise-Valladier, P., Maki, H., Sekiguchi, M., & Fuchs, R. P. P. (1994) *J. Mol. Biol. 236*, 151−164.
Benasutti, M., Ejadi, S., Whitlow, M. D., & Loechler, E. L. (1988) *Biochemistry 27*, 472−481.
Bodenhausen, G., Kogler, H., & Ernst, R. R. (1984) *J. Magn. Reson. 58*, 370−388.
Boelens, R., Scheek, R. M., Dijkstra, K., & Kaptein, R. (1985) *J. Magn. Reson. 62*, 378−386.
Boles, T. C., & Hogan, M. E. (1986) *Biochemistry 25*, 3039−3043.
Bonatti, S., Abbondandolo, A., Corti, G., Fiorio, R., & Mazzaccaro, A. (1978) *Mutat. Res. 52*, 295−300.
Bond, J. A. (1989) *CRC Crit. Rev. Toxicol. 19*, 227−249.
Borer, P. N. (1975) in *Handbook of Biochemistry and Molecular Biology*, CRC Press, Cleveland, OH.
Borgias, B. A., & James, T. L. (1990) *J. Magn. Reson. 87*, 475−487.
Brooks, B. R., Bruccoleri, R. E., Olafson, B. D., States, D. J., Swaminathan, S., & Karplus, M. (1983) *J. Comput. Chem. 4*, 187−217.
Brunger, A. T. (1992) in *X-PLOR, Version 3.1. A System for X-ray Crystallography and NMR*, Yale University Press, New Haven, CT.
Burnouf, D., Koehl, P., & Fuchs, R. P. P. (1989) *Proc. Natl. Acad. Sci. U.S.A. 86*, 4147−4151.
Calladine, C. R. (1982) *J. Mol. Biol. 161*, 343−352.
Cheng, K. C., & Loeb, L. A. (1993) *Adv. Cancer Res. 60*, 121−156.
Cho, B. P., Beland, F. A., & Marques, M. M. (1992) *Biochemistry 31*, 9587−9602.
Cho, B. P., Beland, F. A., & Marques, M. M. (1994) *Biochemistry 33*, 1373−1384.
Comess, K. M., Burstyn, J. N., Essigmann, J. M., & Lippard, S. J. (1992) *Biochemistry 31*, 3975−3990.
Cosman, M., Laryea, A., Fiala, R., Hingerty, B. E., Amin, S., Geacintov, N. E., Broyde, S., & Patel, D. J. (1995) *Biochemistry 34*, 1295−1307.
de Meester, C., Poncelet, F., Roberfroid, M., Rondelet, J., & Mercier, M. (1977) *Mutat. Res. 56*, 147−152.
Dittrich, K. A., & Krugh, T. R. (1991a) *Chem. Res. Toxicol. 4*, 270−276.
Dittrich, K. A., & Krugh, T. R. (1991b) *Chem. Res. Toxicol. 4*, 277−281.
Eckel, L. M., & Krugh, T. R. (1994a) *Nature Struct. Biol. 1*, 89−94.
Eckel, L. M., & Krugh, T. R. (1994b) *Biochemistry 33*, 13611−13624.
Elovaara, E., Engstrom, K., Nakajima, T., Park, S. S., Gelboin, H. V., & Vainio, H. (1991) *Xenobiotica 21*, 651−661.
Feigon, J., Leupin, W., Denny, W. A., & Kearns, D. R. (1983) *Biochemistry 22*, 5943−5951.
Feng, B., & Stone, M. P. (1995) *Chem. Res. Toxicol. 8*, 821−832.
Foureman, G. L., Harris, C., Guengerich, F. P., & Bend, J. R. (1989) *J. Pharmacol. Exp. Ther. 248*, 492−497.
Glickman, B. W., Horsfall, M. J., Gordon, A. J. E., & Burns, P. A. (1987) *Environ. Health Perspect. 76*, 29−32.
Goodman, M. F., Creighton, S., Bloom, L. B., & Petruska, J. (1993) *CRC Crit. Rev. Biochem. 28*, 83−126.
Guengerich, F. P. (1992) *FASEB J. 6*, 745−748.

Guengerich, F. P., Kim, D.-H., & Iwasaki, M. (1991) *Chem. Res. Toxicol. 4*, 168−179.
Hare, D. R., Wemmer, D. E., Chou, S. H., Drobny, G., & Reid, B. R. (1983) *J. Mol. Biol. 171*, 319−336.
Harris, C., Philpot, R. M., Hernandez, O., & Bend, J. R. (1986) *J. Pharmacol. Exp. Ther. 236*, 144−149.
Harris, C. M., Zhou, L., Strand, E. A., & Harris, T. M. (1991) *J. Am. Chem. Soc. 113*, 4328−4329.
Havel, T. F., & Wuthrich, K. (1985) *J. Mol. Biol. 182*, 281−294.
Hodgson, J. T., & Jones, P. D. (1985) *J. Work Environ. 11*, 347−352.
Keepers, J. W., & James, T. L. (1984) *J. Magn. Reson. 57*, 404−426.
Kootstra, A., Lew, L. K., Nairn, R. S., & MacLeod, M. C. (1989) *Mol. Carcinog. 1*, 239−244.
Latham, G. J., & Lloyd, R. S. (1994) *J. Biol. Chem. 269*, 28527−28530.
Latham, G. J., Zhou, L., Harris, C. M., Harris, T. M., & Lloyd, R. S. (1993) *J. Biol. Chem. 268*, 23427−23434.
Latham, G. J., Harris, C. M., Harris, T. M., & Lloyd, R. S. (1995) *Chem. Res. Toxicol. 8*, 422−430.
Loeb, L. A. (1991) *Cancer Res. 51*, 3075−3079.
Madrid, M., Llinas, E., & Llinas, M. (1991) *J. Magn. Reson. 93*, 329−346.
Margulis, L. A., Ibanez, V., & Geacintov, N. E. (1993) *Chem. Res. Toxicol. 6*, 59−63.
Marien, K., Moyer, R., Lovelan, P., Van Holde, K., & Bailey, G. (1987) *J. Biol. Chem. 262*, 7455−7462.
Marion, D., Ikura, M., & Bax, A. (1989) *J. Magn. Reson. 84*, 425−430.
Matanoski, G. M., & Schwarts, L. (1987) *J. Occup. Med. 29*, 675−680.
Miller, J. A. (1970) *Cancer Res. 30*, 559−576.
Moyer, R., Marien, K., Van Holde, K., & Bailey, G. (1989) *J. Biol. Chem. 264*, 12226−12231.
Muench, K. F., Misra, R. P., & Humayun, M. Z. (1983) *Proc. Natl. Acad. Sci. U.S.A. 80*, 6−10.
Nakajima, T., Elovaara, E., Gonzalez, F. J., Gelboin, H. V., Raunio, H., Pelkonen, O., Vainio, H., & Aoyama, T. (1994a) *Chem. Res. Toxicol. 7*, 891−896.
Nakajima, T., Wang, R.-S., Elovaara, E., Gonzalez, F. J., Gelboin, H. V., Vainio, H., & Aoyama, T. (1994b) *Biochem. Pharmacol. 48*, 637−642.
Nelson, D. R., Kamataki, T., Waxman, D. J., Guengerich, F. P., Estabrook, R. W., Feyereisen, R., Gonzalez, F. J., Coon, M. J., Gunsalus, I. C., Goto, O., Okuda, K., & Nebert, D. W. (1993) *DNA Cell Biol. 10*, 1−51.
Nilsson, L., & Karplus, M. (1986) *J. Comput. Chem. 7*, 591−616.
Nilsson, L., Clore, G. M., Gronenborn, A. M., Brunger, A. T., & Karplus, M. (1986) *J. Mol. Biol. 188*, 455−475.
Norppa, H., Sorsa, M., Pfaffli, P., & Vainio, H. (1980) *Carcinogenesis 1*, 357−361.
Norppa, H., Hemminki, K., Sorsa, M., & Vainio, H. (1981) *Mutat. Res. 91*, 243−250.
Osborne, M. R. (1990) *Chem.-Biol. Interact. 75*, 131−140.
Ott, M. G., Kolesar, R. C., Schamweber, H. C., Schneider, E. J., & Venable, J. R. (1980) *J. Occup. Med. 22*, 445−460.
Patel, D. J., Kozlowski, S. A., Ikuta, S., Itakura, K., Bhatt, R., & Hare, D. R. (1982) *Cold Spring Harbor Symp. Quant. Biol. 97*, 197−206.
Patel, D. J., Shapiro, L., & Hare, D. (1987) *Q. Rev. Biophys. 20*, 35−112.
Plateau, P., & Gueron, M. (1982) *J. Am. Chem. Soc. 104*, 7310−7311.
Quintanilla, M., Brown, K., Ramsden, M., & Balmain, A. (1986) *Nature 322*, 78−80.
Randall, S. K., Eritja, R., Kaplan, B. E., Petruska, J., & Goodman, M. F. (1987) *J. Biol. Chem. 262*, 6864−6870.
Ravishankar, G., Swaminathan, S., Beveridge, D. L., Lavery, R., & Sklenar, H. (1989) *J. Biomol. Struct. Dyn. 6*, 669−699.
Refolo, L. M., Conley, M. P., Sambamurti, K., Jacobsen, J. S., & Humayun, M. Z. (1985) *Proc. Natl. Acad. Sci. U.S.A. 82*, 3096−3100.
Reid, B. R. (1987) *Q. Rev. Biophys. 20*, 2−28.
Rodriguez, H., & Loechler, E. L. (1993) *Biochemistry 32*, 1759−1769.
Ryckaert, J.-P., Ciccotti, G., & Berendsen, H. J. C. (1977) *J. Comput. Phys. 23*, 327−341.
Savela, K., & Hemminki, K. (1986) *Arch. Toxicol., Suppl. 9*, 281−285.
Schurter, E. J., Yeh, H. J. C., Sayer, J. M., Lakshman, M. K., Yagi, H., Jerina, D. M., & Gorenstein, D. G. (1995) *Biochemistry 34*, 1364−1375.
Shibutani, S. (1993) *Chem. Res. Toxicol. 6*, 625−629.
Shibutani, S., & Grollman, A. P. (1993) *J. Biol. Chem. 268*, 11703−11710.
Shibutani, S., Takeshita, M., & Grollman, A. P. (1991) *Nature 349*, 431−434.
Singer, B., Chavez, F., Goodman, M. F., Essigmann, J. M., & Dosanjh, M. K. (1989) *Proc. Natl. Acad. Sci. U.S.A. 86*, 8271−8274.
Sklenar, V., Brooks, B. R., Zon, G., & Bax, A. (1987) *FEBS Lett. 216*, 249−252.
Topal, M. D. (1988) *Carcinogenesis 9*, 691−696.
Topal, M. D., Eadie, J. S., & Conrad, M. (1986) *J. Biol. Chem. 261*, 9879−9885.
Voigt, J. M., & Topal, M. D. (1990) *Biochemistry 29*, 5012−5018.
Voigt, J. M., Van Houten, B., Sancar, A., & Topal, M. D. (1989) *J. Biol. Chem. 264*, 5172−5176.
Vousden, K. H., Bos, J. L., Marshall, C. J., & Phillips, D. H. (1986) *Proc. Natl. Acad. Sci. U.S.A. 83*, 1222−1226.
Wade, D. R., Airy, S. C., & Sinsheimer, J. E. (1978) *Mutat. Res. 58*, 217−223.
Wilson, W. D., Ratmeyer, L., Zhao, M., Strekowski, L., & Boykin, D. (1993) *Biochemistry 32*, 4098−4104.
Wong, O. (1990) *J. Ind. Med. 47*, 753−762.
Wuthrich, K. (1986) in *NMR of Proteins and Nucleic Acids*, John Wiley & Sons, New York.
Wuthrich, K., & Wagner, G. (1978) *Trends Biochem. Sci. 3*, 227−230.
Zarbl, H., Sukumar, S., Arthuyr, A. V., Martin-Zanca, D., & Barbacid, M. (1985) *Nature 315*, 382−385.

BI942991X